CrossMark

Computational Modeling of Arc–Slag Interaction in DC Furnaces

QUINN G. REYNOLDS[1,2]

1.—Pyrometallurgy Division, Mintek, Rabdburg 2194, South Africa. 2.—e-mail: quinnr@mintek.co.za

The plasma arc is central to the operation of the direct-current arc furnace, a unit operation commonly used in high-temperature processing of both primary ores and recycled metals. The arc is a high-velocity, high-temperature jet of ionized gas created and sustained by interactions among the thermal, momentum, and electromagnetic fields resulting from the passage of electric current. In addition to being the primary source of thermal energy, the arc jet also couples mechanically with the bath of molten process material within the furnace, causing substantial splashing and stirring in the region in which it impinges. The arc's interaction with the molten bath inside the furnace is studied through use of a multiphase, multiphysics computational magnetohydrodynamic model developed in the OpenFOAM® framework. Results from the computational solver are compared with empirical correlations that account for arc–slag interaction effects.

INTRODUCTION

Direct-current (DC) plasma arc furnaces are used extensively in the pyrometallurgical production of steel, ferrochromium, ferronickel, titanium dioxide, and other valuable materials.[1] A typical DC arc furnace is shown in schematic form in Fig. 1. The furnace vessel consists of a cylindrical steel shell mounted on a flat or domed base, and it is covered with a conical roof. The vessel is lined with thermally insulating refractory material to contain the molten bath of process material inside, which typically consists of at least two immiscible phases—a dense metal phase and a lighter metal-oxide slag phase. These molten phases are maintained at temperatures between 1500°C and 2000°C. Electrical power from the grid is converted from alternating to direct current using solid-state rectifiers, and it is passed through the unit via one or more graphite electrodes that enter through the roof of the vessel. When the circuit is completed, a plasma arc discharge forms in the gas space between the tip of the electrode and the surface of the molten bath.

The plasma arc is the "engine room" of the DC arc furnace, providing thermal and mechanical energy to ensure that the materials in the molten bath are kept at high temperature and well mixed. Understanding the arc's interaction with the multiphase fluid in the bath is important for design and scale-up of furnaces from pilot (< 3 MW) to industrial

(> 50 MW) scales as it is the geometry of the bath surface beneath the arc jet[2,3] that determines many of the primary electrical characteristics of the system—for example, the nonlinear, nonohmic resistances in the arc and slag bath that are required to design the furnace power supply.

Prior to this work, efforts to characterize the effect of arc–slag interaction on the mechanical and electrical behavior of the furnace have used primarily empirical methods.[3,4] Approximate computational modeling approaches based on theoretically estimated values of the thrust force generated by the arc jet have been attempted but generally consider only the multiphase fluid flow physics in the molten bath.[5] Such models can estimate the dimensions of the cavity formed in the molten bath by the mechanical force exerted by arc jet, but they cannot calculate the electrical behavior of the arc and slag directly. In contrast, full magnetohydrodynamic models of the plasma phase have been developed[6] and permit detailed study of the rapid, chaotic dynamic and electrical response of the arc, but these do not take into account the evolution of the bath surface to which it attaches.

Development of a model incorporating both multiphase fluid flow and electromagnetic phenomena was therefore deemed to be of some value in improving fundamental understanding of the complex interactions between the plasma arc and the molten bath in DC furnaces.
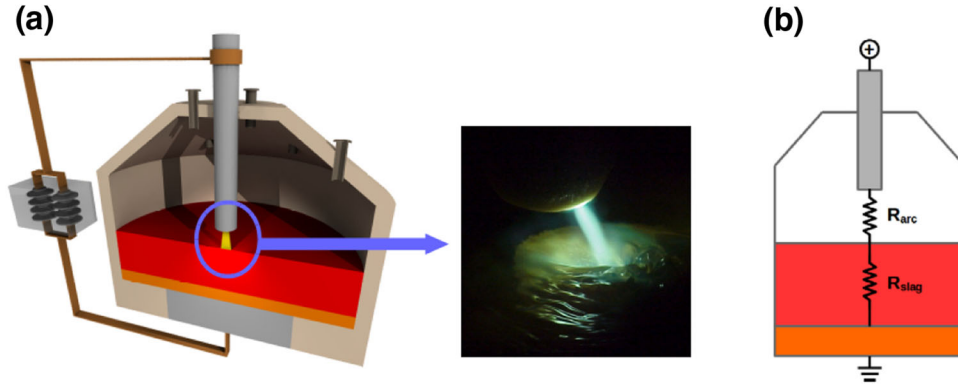
Fig. 1. (a) Schematic of DC arc furnace with a photograph of the arc and (b) simplified furnace circuit diagram show slag and arc elements. Photograph republished by permission of Mintek.

DESCRIPTION OF COMPUTATIONAL MODEL

To develop an improved computational model of the interaction between the arc and the molten bath, four physical phenomena must be accounted for—momentum transfer, heat transfer, electromagnetism, and phase separation. These are expressed in the form of standard conservation equations with the appropriate coupling and source terms.[4,6] Phase separation is handled using the volume-of-fluid (VOF) method,[7] in which a set of phase fields α_n $(0 < \alpha_n < 1)$ define the extent of each phase n. The constitutive equations for the system are shown in Eqs. 1–5 using only two phases described by a single phase fraction α for brevity:

$$\frac{\partial(\rho\mathbf{u})}{\partial t} + \nabla \times (\rho\mathbf{u}\mathbf{u}) + \nabla P = \nabla \cdot \tau_{\mathbf{ij}}$$
$$- \gamma\nabla \times \left(\frac{\nabla\alpha}{|\nabla\alpha|}\right)\nabla\alpha + \mathbf{j} \times \nabla \times \mathbf{A} - \rho\mathbf{g} \quad (1)$$

$$\frac{\partial\rho}{\partial t} + \nabla \times (\rho\mathbf{u}) = 0 \quad (2)$$

$$\frac{\partial\alpha}{\partial t} + \nabla \times (\alpha\mathbf{u}) = 0 \quad (3)$$

$$\frac{\partial(\rho C_\mathrm{P}T)}{\partial t} + \nabla \times (\rho C_\mathrm{P}\mathbf{u}T) =$$
$$\nabla \times \left(k\nabla T + \frac{5k_B\mathbf{j}}{2e}T\right) + \frac{\mathbf{j} \times \mathbf{j}}{\sigma} - Q_\mathrm{R} \quad (4)$$

$$\mathbf{j} = -\sigma\left(\nabla\phi + \frac{\partial\mathbf{A}}{\partial t} - \mathbf{u} \times \nabla \times \mathbf{A}\right)$$
$$\nabla \times \mathbf{j} = 0 \nabla^2 \quad \mathbf{A} = -\mu_0\mathbf{j} \quad (5)$$

In these expressions, ρ is the phase mixture density, $\mathbf{u}$ is the velocity vector, P is the pressure, $\tau_{\mathbf{ij}}$ is the viscous stress tensor, γ is the surface tension between the phases, $\mathbf{g}$ is the gravity vector, T is the fluid temperature, C_P is the heat capacity of the phase mixture, k is the thermal conductivity of the phase mixture, k_B is the Boltzmann constant, e is the electron charge, Q_R is the net thermal radiation emission coefficient (a function of temperature and plasma gas), σ is the electrical conductivity of the phase mixture, $\mathbf{j}$ is the electric current density vector, $\mathbf{A}$ is the magnetic vector potential, ϕ is the electric potential field, and μ_0 is the magnetic permeability of the phase mixture.

Assumptions made for the solution of Eqs. 1–5 include incompressible flow in all phases and a Coulomb gauge on the magnetic vector potential field. Local thermodynamic equilibrium is also assumed in the plasma phase, permitting bulk physical properties in this phase to be defined as functions of temperature.[8] At the phase interfaces, physical properties are calculated as linear combinations of the individual phase values, weighted by the phase fractions. In the present work, the region is modeled as a two-dimensional slice; nevertheless, the algorithm extends naturally to three dimensions if sufficient computational resources are available.

An example of the model geometry and mesh used for the numerical solution is shown in Fig. 2. Boundary conditions are imposed at the perimeter of the mesh for each field to be solved. At the "sidewall" surface, a no-slip condition is used for Eqs. 1 and 2, a zero gradient condition for Eq. 3, a fixed temperature (2000 K) condition for Eq. 4, and an electrically insulating condition for Eq. 5. The "hearth" surface uses the same conditions as for "sidewall" but with a ground-potential condition for Eq. 5. At the "freeboard" surface, a total pressure inlet–outlet condition is used for Eqs. 1 and 2, velocity-based inlet–outlet conditions for Eqs. 3 and 4, and an electrically insulating condition for Eq. 5. At the "electrode" surface, a no-slip condition is used for Eqs. 1 and 2, a zero gradient condition for Eq. 3, a fixed temperature (4000 K) condition for Eq. 4, and an electrically insulating condition for Eq. 5. The "cathode spot" surface uses the same conditions as for "electrode" but with a fixed current density condition for Eq. 5 based on thermionic emission from hot graphite surfaces.[3]
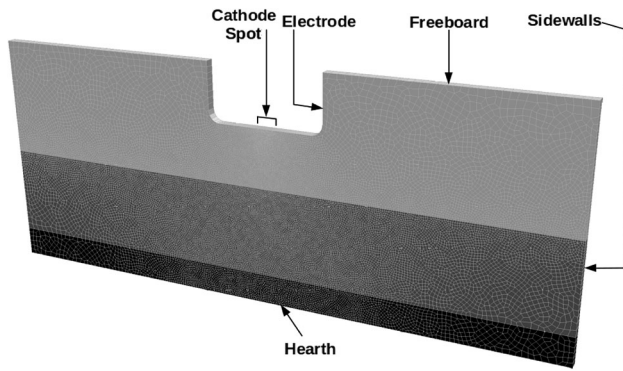
Fig. 2. Example model region shows numerical mesh and boundary locations.

A finite volume method solver based on the governing equations was developed in the Open-FOAM® 4.0 open-source computational modeling framework.[9] The standard "compressibleMultiPhaseInterFoam" solver was extended with a phase thermodynamic model based on lookup tables to be able to account for the highly nonlinear temperature dependence of the physical and thermodynamic properties of the plasma phase, together with an iterative solution of Maxwell's equations for the electric and magnetic fields. The multiphase VOF method together with OpenFOAM's MULES limiter scheme was used to capture phase separation effects. Unstructured computational meshes were generated using Gmsh 2.10.1.[10]

RESULTS AND DISCUSSION

To study the physical and electrical behavior of the multiphase plasma arc model, several test cases representing a small-scale DC furnace pilot plant were constructed and executed. The parameters used for these test cases are shown in Table I. Arc length and furnace current were varied between the test cases to examine the effect of these important control variables on the system.

All models were run for 1000 ms, starting from initial conditions of zero velocity and constant temperature (7500 K in the plasma phase, 2000 K elsewhere). Surface tension effects were assumed to be secondary to momentum and buoyancy forces in this study, and as a result, the surface tension among the slag, metal, and plasma phases was set at a low value (0.07 N/m). In reality, this value is considerably higher (typically 0.5–1 N/m for slag–metal systems); solutions using such high values are possible, but special care must be taken with the treatment of the surface tension term in Eq. 1 and the solution of Eq. 3 to avoid numerical instability and unrealistic artifacts at the interfaces.

Mechanical Interaction Effects

As a result of the force exerted by the high-velocity arc jet, a cavity or depression is generally formed in the liquid surface of the slag beneath the electrode. It is of interest to operators and designers to understand the size and shape of this cavity as it has some bearing on the metallurgical and electrical performance of the furnace.

The mechanical interaction between the arc and bath is shown visually in selected results from the computational models in Figs. 3 and 4. In these figures, the scale for the temperature field is 2000 K (light gray) to 15,000 K (black).

It can be observed that at shorter arc lengths and higher currents, the interaction between the plasma arc and the slag bath is considerably stronger. A larger cavity is formed in the bath surface, and the resulting flow produces waves and splashing in the vicinity of the arc's attachment point. Deformation of the surface also feeds back into the plasma phase to some degree, causing additional flow and electromagnetic instabilities in the arc column.

The dimensions of the deformation in the slag bath surface produced by the arc may be quantified in terms of the theory of turbulent jets impinging on liquid surfaces as developed by Cheslak et al.[12] and others. This theory was verified computationally by Forrester and Evans[13] and Nguyen and Evans[14] for planar and round turbulent jets, respectively, with reasonably good agreement found. The relevant nondimensional relationships from the theory are shown in Eq. 6 for round jets and in Eq. 7 for planar jets:

$$N_{\mathrm{Fr}} = \frac{T}{g\rho_S L_A^3} = \frac{\pi}{2K_R}\frac{a}{L_A}\left(1 + \frac{a}{L_A}\right)^2 \quad (6)$$

$$N_{\mathrm{Fr}} = \frac{T}{g\rho_S L_A^3} = \frac{2}{K_P}\frac{a}{L_A}\left(1 + \frac{a}{L_A}\right) \quad (7)$$

Here, T is the thrust force generated by the arc (related to the furnace current I by $T = 1.663 \times 10^{-7} I^2$),[5] L_A is the arc length (clearance between electrode tip and slag surface), K_R and K_P are turbulent jet centerline velocity decay constants for the round and planar cases (with typical values 5.3 and 2.5, respectively),[5,13] and a is the depth of the cavity relative to the quiescent slag surface.

Cavity depth was estimated from the multiphase plasma arc computational model results by identifying the location of the slag–plasma interface along the furnace centerline at each time step. All time steps in the final 500 ms of the model run were then analyzed statistically to determine the average cavity depth, as well as the minimum and maximum range of cavity depths in which the model spends 90% of its time. The results from all model cases are shown in Fig. 5 when compared against Eqs. 6 and 7.

In general, the computational multiphase plasma arc model results match well with the theory of turbulent jet impingement. This alignment is perhaps somewhat unsurprising as several workers[3,15]

Table I. Key parameters used in computational models

| Parameter	Value	Parameter	Value
Furnace diameter	0.5 m	Arc lengths	0.05 m, 0.075 m, 0.1 m
Electrode diameter	0.1 m	Currents	0.5 kA, 0.75 kA, 1 kA
Metal depth	0.025 m	Slag depth	0.075 m
Metal density	7000 kg/m^3	Slag density	3500 kg/m^3
Metal viscosity	6×10^{-3} Pa.s	Slag viscosity	0.1 Pa.s
Metal conductivity (σ)	10^6 S/m	Slag conductivity (σ)	66.7 S/m
Metal heat capacity	820 J/kg/K	Slag heat capacity	1000 J/kg.K
Metal conductivity (k)	36 W/mK	Slag conductivity (k)	5 W/mK
Plasma gas data	Air[8,11]	Cathode spot **j**	2×10^7 A/m^2
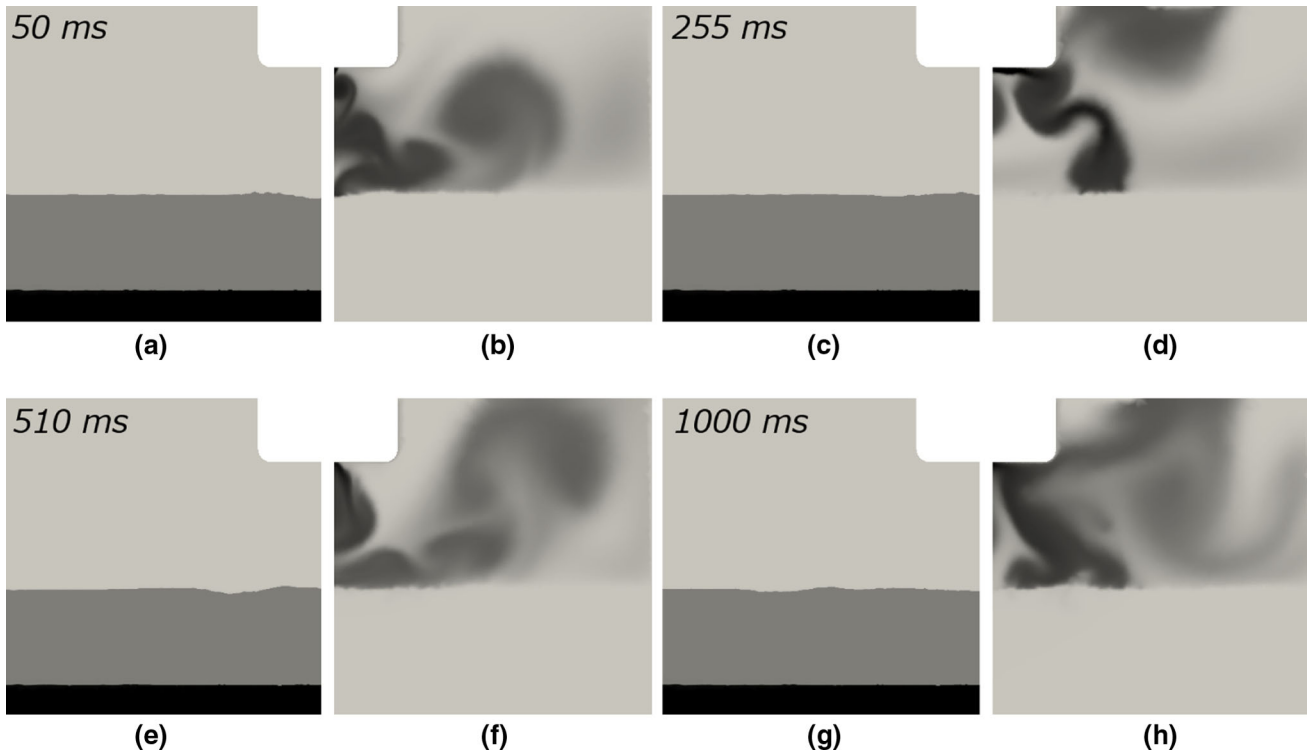
Fig. 3. Computational model results for the case of 0.5-kA current and 10-cm arc length. (a), (c), (e), and (g) show phase field, whereas (b), (d), (f), and (h) show temperature field scaled between 2000 K (gray) and 15,000 K (black).

have identified similarities between the plasma arc and the turbulent jet in terms of its time-averaged shape and structure. It does, however, confirm that in the absence of experimental data or computational model results, it is possible to use relationships such as Eqs. 6 and 7 to generate rough estimates of the dimensions of the slag cavity formed by arcs in DC furnaces as a function of arc length and current.

Electrical Interaction Effects

DC furnaces are primarily electrically powered devices, and an understanding of the electrical behavior of the coupled arc–slag system is critical for their correct design and operation. In certain cases, the slag volume is negligible or is blown into a foam of such low density that the arc penetrates through it directly to the metal. Nevertheless, in typical DC smelting processes, the presence of a slag layer is a metallurgical necessity. The slag's resistance to the flow of electricity can then contribute significantly to the total furnace voltage at a given current, in addition to the voltage drop across the arc. These effects have been examined previously using semi-empirical models of arc and bath,[3,4] and it is possible to match these correlations well enough to operational furnace data for them to be of some value as design tools.

Total furnace voltage was determined from the computational model cases by finding the maximum value of the electric potential field ϕ at every time
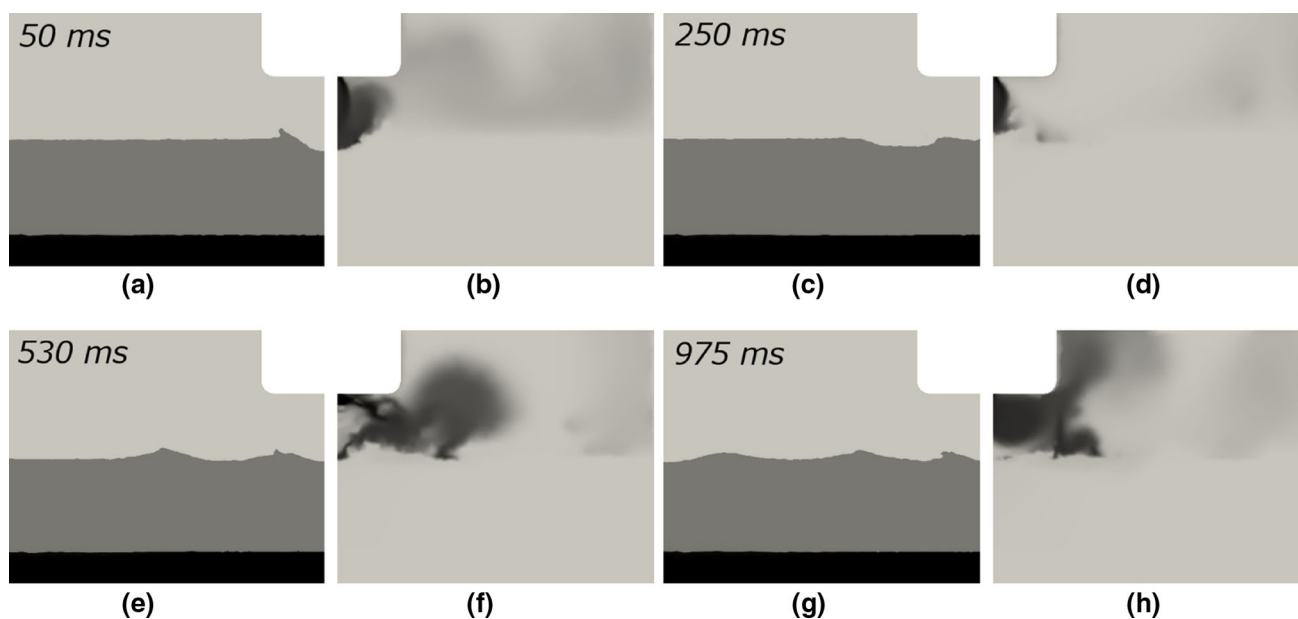
Fig. 4. Computational model results for case of 0.75-kA current and 5-cm arc length. (a), (c), (e), and (g) show phase field, whereas (b), (d), (f), and (h) show temperature field scaled between 2000 K (gray) and 15,000 K (black).
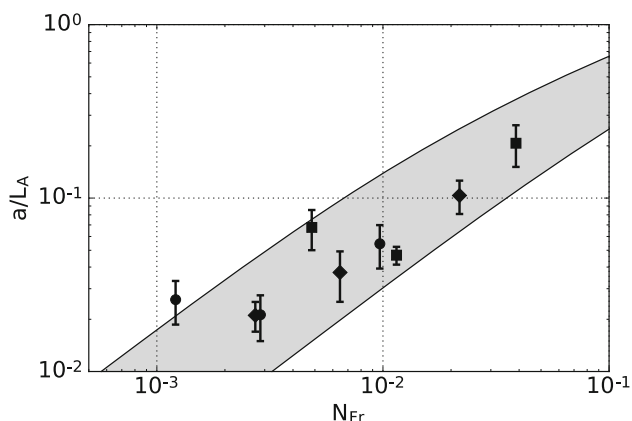

Fig. 5. Computational model results (black circle 0.5 kA, black diamond 0.75 kA, black square 1 kA) with 90% confidence range shown by bars, compared against range defined by Eqs. 6 and 7 (gray area).

step for the last 500 ms of the simulation. This instantaneous voltage was then analyzed statistically to find the average as well as the 90% probability range. The results are shown in Fig. 6 when compared with furnace voltage calculations using the values in Table I together with the semi-empirical methodology described in Ref. [4].

There is a considerable difference in the absolute voltages predicted; nonetheless, it should be noted that the empirical calculations are somewhat conservative in nature and tend to overpredict furnace voltage. In addition, slag conduction is a highly three-dimensional problem, and it is likely that the two-dimensional planar computational models in use here are causing appreciable quantitative error in the modeled results. It is, however, promising to

observe that the computational model results (mostly) capture the correct trends, with voltage increasing regularly as arc length is increased, at a rate that matches the empirical trends.

It is interesting to observe the large range of voltages traversed by the computational models; in many cases, peak voltages of more than double the average are observed. This is a result of the rapid and highly chaotic dynamics of the plasma arc, particularly at longer arc lengths and higher currents. Interaction with the slag bath can exacerbate this instability, as shown in Figs. 7 and 8. The current density in Fig. 8 is scaled between 0 (light gray) and 10^7 A/m² (black).

Figure 8 shows that at around 570 ms into the model, splashing of slag from the cavity underneath the electrode causes small droplets of slag to enter the arc column. Because they are at a low temperature compared with the arc, these droplets rapidly cool the plasma in their immediate vicinity and drastically reduce its electrical conductivity. This causes the "holes" in the current density field observed in Fig. 8 and the rapid spike in furnace voltage observed in Fig. 7. As the droplets have a much higher density than the surrounding plasma, they also interfere with the flow field of the arc, breaking the column up into many thinner filaments. This flow instability then feeds back into the temperature field and the electrical behavior, causing additional fluctuations in the voltage.

CONCLUSION

Coupling of a magnetohydrodynamic plasma arc solver to an existing multiphase fluid flow solver was successfully achieved, resulting in a
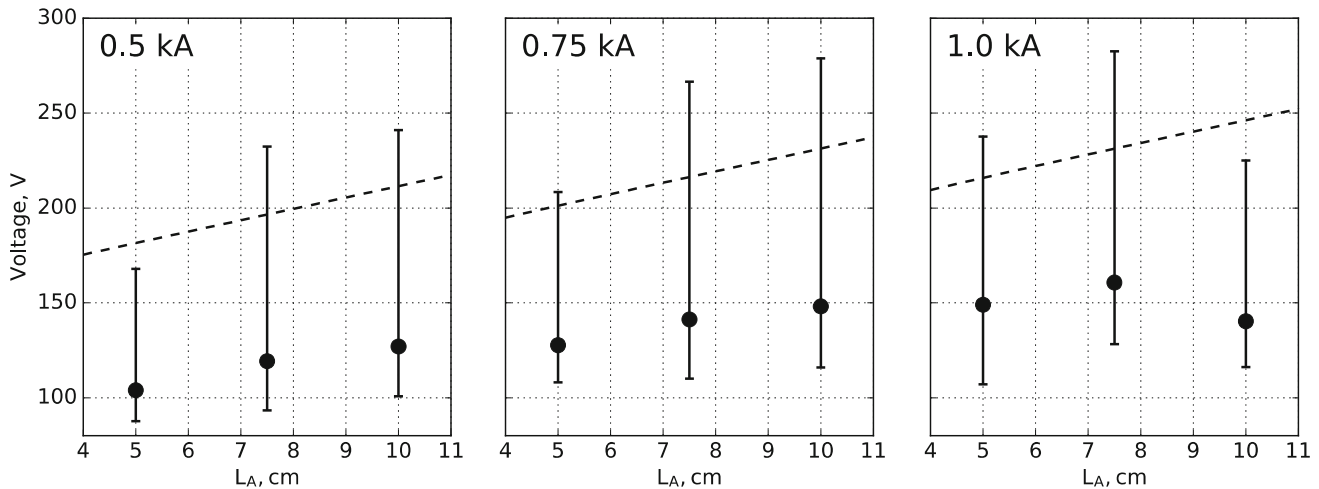
Fig. 6. Furnace voltages at different currents and arc lengths from computational model (filled circle) and empirical calculations (dashed lines).
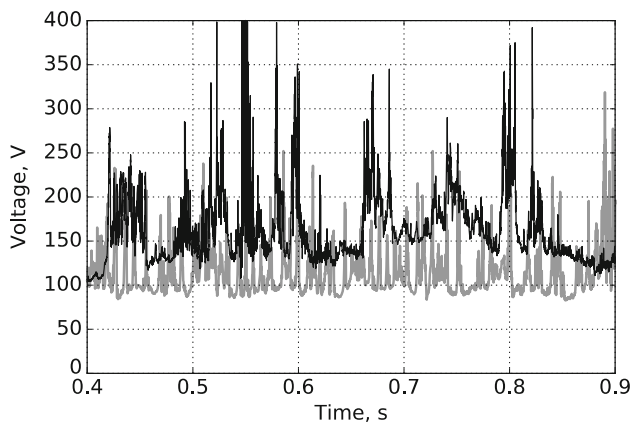

Fig. 7. Evolution of average voltage for 5-cm arc lengths: 0.5-kA current (gray) and 1-kA current (black).
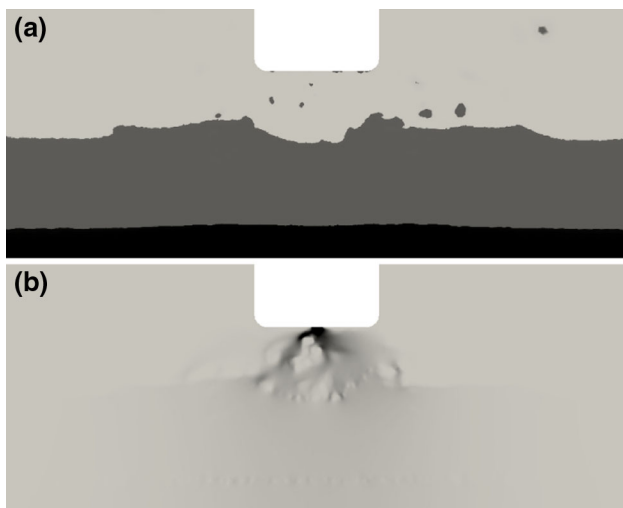

Fig. 8. (a) phase field and (b) current density field at 570 ms, 5-cm arc length, and 1-kA current.

computational model able to capture some of the complex physical behavior and dynamics of the arc–bath interaction zone inside DC arc furnaces. Reasonable agreement was found between the present model and theoretical relationships from turbulent jet theory for the dimensions of the cavity formed by the arc in the molten slag layer. Comparison of the model results with semi-empirical correlations used to calculate the electrical parameters of DC furnaces showed that although the correct trends were captured, the values of the predicted voltages in the computational model were lower.

Much future work is possible in this area to extend and enhance the multiphase plasma arc computational model. Most immediately, extending the models to three dimensions would eliminate much of the uncertainty around the accuracy of the electrical calculation in particular. The dynamics of the fluid flow and heat transfer in the arc and slag cavity are also likely to be more physically realistic in three dimensions. To model industrial-scale DC furnaces, inclusion of an appropriate turbulence model (LES or DES is suggested) will be required to avoid prohibitively large computational meshes. Finally, more detailed descriptions of the plasma, slag, and metal physical properties in terms of temperature would help to improve the model's quantitative predictions.

ACKNOWLEDGEMENTS

REFERENCES

1. R.T. Jones and T.R. Curr, *Proceedings of Southern African Pyrometallurgy 2006*, ed. By R.T. Jones (SAIMM, Johannesburg, 2006), p. 127.

2. R.T. Jones, Q.G. Reynolds, and M.J. Alport, *Miner. Eng.* 15, 985 (2002).
3. B. Bowman, *Proceedings of the 52nd Electric Furnace Conference*, ed. Iron and Steel Society (Iron and Steel Society, Nashville TN, 1994), p. 111.
4. Q.G. Reynolds and R.T. Jones, *J. South Afr. Inst. Min. Metall.* 104, 345 (2004).
5. Q.G. Reynolds, *Proceedings of the 9th South African Conference on Computational and Applied Mechanics*, ed. By J. Hoffman (SAAM, Stellenbosch, 2014), p. 58.
6. Q.G. Reynolds, R.T. Jones, and B.D. Reddy, *J. South Afr. Inst. Min. Metall.* 110, 733 (2010).
7. C.W. Hirt and B.D. Nichols, *J. Comput. Phys.* 39, 201 (1981).
8. M.I. Boulos, P. Fauchais, and E. Pfender, *Thermal Plasmas: Fundamentals and Applications*, Vol. 1 (New York NY: Plenum Press, 1994), p. 413.
9. H.G. Weller, G. Tabor, H. Jasak, and C. Fureby, *Comput. Phys.* 12, 640 (1998).
10. C. Geuzaine and J.-F. Remacle, *Int. J. Numer. Methods Eng.* 79, 1309 (2009).
11. Y. Naghizadeh-Kashani, Y. Cressault, and A. Gleizes, *J. Phys. D Appl. Phys.* 35, 2925 (2002).
12. F.R. Cheslak, J.A. Nicholls, and M. Sichel, *J. Fluid Mech.* 36, 55 (1969).
13. S.E. Forrester and G.M. Evans, *Proceedings of the 1st International Conference on CFD in the Mineral and Metal Processing and Power Generation Industries*, ed. CSIRO (CSIRO, Melbourne, Australia, 1997) p. 313.
14. A.V. Nguyen and G.M. Evans, *Appl. Math. Model.* 30, 1472 (2006).
15. M. Ushio, J. Szekely, and C.W. Chang, *Ironmak. Steelmak* 8, 279 (1981).